Temperature- and size-dependent characteristics in ultrathin inorganic light-emitting diodes assembled by transfer printing

Tae-il Kim,[1,2,a)] Soo Hyun Lee,[3,a)] Yuhang Li,[4,5] Yan Shi,[6,4] Gunchul Shin,[7] Sung Dan Lee,[7] Yonggang Huang,[4] John A. Rogers,[7,8,b)] and Jae Su Yu[3,b)]

[1]*School of Chemical Engineering, Sungkyunkwan University (SKKU), Suwon 440-746, South Korea*
[2]*IBS Center for Neuroscience Imaging Research (CNIR), Institute for Basic Science (IBS), Daejeon 305-701, South Korea*
[3]*Department of Electronics and Radio Engineering, Kyung Hee University, 1 Seocheon-dong, Giheung-gu, Yongin-si, Gyeonggi-do 446-701, South Korea*
[4]*Department of Civil and Environmental Engineering, Department of Mechanical Engineering, Center for Engineering and Health, and Skin Disease Research Center, Northwestern University, Evanston, Illinois 60208, USA*
[5]*Department of Engineering Mechanics, Soft Matter Research Center, Zhejiang University, Hangzhou 310027, China*
[6]*State Key Laboratory of Mechanics and Control of Mechanical Structures, Nanjing University of Aeronautics and Astronautics, Nanjing 210016, China*
[7]*Seitz Materials Research Laboratory, Department of Materials Science and Engineering, University of Illinois at Urbana-Champaign, Urbana, Illinois 61801, USA*
[8]*Department of Electrical and Computer Engineering, Department of Mechanical Science and Engineering, Department of Chemistry, and Beckman Institute for Advanced Science and Technology, University of Illinois at Urbana-Champaign, Urbana, Illinois 61801, USA*

(Received 24 December 2013; accepted 18 January 2014; published online 3 February 2014)

Favorable temperature- and size-dependent device characteristics in mechanically flexible, thin (~6.45 μm thick), microscale inorganic InGaN/GaN-based light-emitting diodes enable their use as highly efficient, robust devices that are capable of integration on diverse classes of unconventional substrates, including sheets of plastic. Finite element analysis and systematic studies of the operational properties establish important thermal, electrical, and optical considerations for this type of device. © *2014 AIP Publishing LLC*. [http://dx.doi.org/10.1063/1.4863856]

Recent research in materials and device engineering demonstrates ability to use various organic and inorganic semiconductors in mechanically flexible and deformable electronics for wearable and bio-integrated devices.[1–5] Organic light emitting diodes (OLEDs), in particular, offer strong potential for use in flexible display. Remaining areas for improvement are in efficiency and lifetime of operation, and in simplified schemes for encapsulation.[6] For certain applications, such as bio-integrated light sources in optogenetics[5,7] and other areas,[8–12] ultrathin, flexible inorganic light-emitting diodes with microscale lateral dimensions (μ-ILEDs) could provide attractive alternatives.[5,7–12] Such classes of devices can be fabricated by epitaxial growth and processing on a source wafer, followed by undercut etching[10,13] or laser lift off (LLO)[14–16] and transfer printing[17] to a substrate of interest. Although such classes of devices exhibit superior performance and stability, the efficiencies can be degraded and the emission spectra can shift due to difficulties in thermal management, particularly for substrates such as plastics that have poor thermal conductivity.[13,14,16] This letter explores these and related fundamental effects, through temperature- and size-dependent behaviors in μ-ILEDs on plastic.

Figs. 1(a)–1(d) outlines the process for fabricating flexible inorganic InGaN/GaN-based μ-ILEDs via transfer printing. The first step involves formation of thin (~6.45 μm thick) layers of active materials grown on sapphire substrates, subsequently released by LLO. The devices use 200 nm p-GaN/140 nm multiple quantum wells (MQW)/400 nm spacer/2 μm n-GaN/3.8 μm undoped GaN buffer layers with n- and p-contacts (25×25 μm^2 square Cr/Au (15 nm/300 nm) metal pads) and a partially transparent p-current spreading layer (*L*-shape patterned Ni/Au (15 nm/15 nm)). Bilayers metal (Ni 15 nm and Au 15 nm) formed by sputter deposition onto p-doped GaN are patterned into an L-shape by photolithography and wet etching. Annealing in an oxygen and nitrogen atmosphere at 500 °C for 10 min enhances transparency and electrical contact properties. (Detailed procedures appear elsewhere.[14]) Release of the resulting μ-ILEDs onto the structured surface of a slab of polydimethylsiloxane (PDMS, with an array of vertical pillars with 3 μm diameter, 1.2 μm height, and 5 μm spacing) (Fig. 1(a)) prepares the devices for transfer printing. For present purposes, PDMS stamps with raised features of relief matched to the targeted μ-ILEDs (i.e., 100×100 μm^2 post with 100 μm height PDMS stamp for 100×100 μm^2 μ-ILED), allow the devices to be printed onto sheets of poly(ethylene terephthalate) (PET, 50 μm thick; Grafix Dura-Larfilm roll) coated with a thin photocurable adhesive. Photolithography and wet etching using a photosensitive benzocyclobutene (6 μm thick; photocurable BCB) and Cr (15 nm)/Au (300 nm) layer as a resist (Fig. 1(d)), form contacts and interconnects. An image of a representative device (1×1 mm^2) appears in Fig. 1(f).

[a)]T.-i. Kim, S. H. Lee contributed equally to this work.
[b)]Authors to whom correspondence should be addressed. Electronic addresses: jrogers@illinois.edu and jsyu@khu.ac.kr.

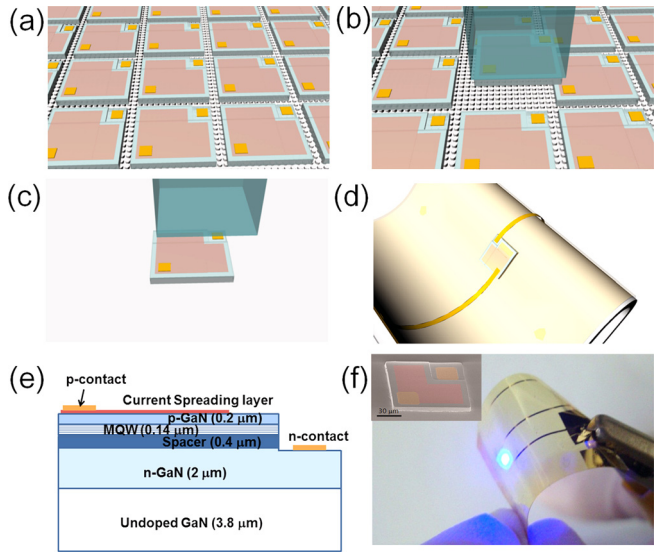

FIG. 1. Schematic illustrations of the process steps for forming flexible μ-ILEDs by transfer printing, including (a) fabrication of μ-ILEDs with various chip sizes of $100 \times 100\ \mu m^2$, $300 \times 300\ \mu m^2$, $500 \times 500\ \mu m^2$, and $1 \times 1\ mm^2$ and arrays on the structured PDMS slabs, (b) selectively retrieving single μ-ILEDs using PDMS stamps and (c) printing on to a flexible substrate, and (d) forming passivation followed by metal interconnection. The structured layers of μ-ILEDs are shown in (e). A representative $1 \times 1\ mm^2$ μ-ILED printed on a 50 μm thick PET substrate is shown in (f). The radius of bending curvature is about 5 mm.

Device sizes range from $100 \times 100\ \mu m^2$ up to dimensions of $1 \times 1\ mm^2$ by use of different patterns formed by photolithography and etching in the fabrication process.[14]

Fig. 2(a) shows the light-current-voltage (L-I-V) curves measured using flexible μ-ILEDs with various sizes at 298 K. As the injection current increases, the optical output power (P_{opt}) of each device increases without significant degradation until a saturation point caused by device heating. With increasing size, higher injection currents are possible, thereby allowing improved maximum P_{out}, due simply to the increased emitting volume, as expected based on the behavior of conventional devices on sapphire substrates.[18,19] The maximum values of P_{out} are 0.09 mW at 4 mA ($J = 40.00\ A/cm^2$), 0.24 mW at 8 mA ($J = 8.89\ A/cm^2$), 0.31 mW at 9 mA ($J = 3.60\ A/cm^2$), and 0.52 mW at 18 mA ($J = 1.80\ A/cm^2$) for devices with dimensions of $100 \times 100\ \mu m^2$, $300 \times 300\ \mu m^2$, $500 \times 500\ \mu m^2$, and $1 \times 1\ mm^2$, respectively. The turn-on voltages ($\sim$3 V) do not vary with size (Fig. 2(a)), indicating proper behavior of the current spreading layer and *L*-shaped ohmic contact. Changes in temperature alter the bandgap of the material[20,21] and other parameters that determine the operation characteristics. Fig. 2(b) shows the temperature change, ΔT, in the μ-ILEDs determined by the finite element method (FEM)[22] as a function of the injection power, for the case of steady-state behavior in devices with various sizes. The temperature distribution across the μ-ILED is approximately uniform[23,24] because its thermal conductivity, 160 W/m/K,[24] is orders of magnitude larger than that of the other associated materials, BCB (0.3 W/m/K[14]), PET (0.15 W/m/K[14]), PDMS (0.15 W/m/K[25]), and glass (1.4 W/m/K[26]). The model assumes that the bottom surface of the glass is at ambient temperature and that the top surface of the BCB undergoes natural heat convection with a convection coefficient of 25 $W/m^2/K$.[27] The ratio of injection power to the volume of the μ-ILED gives the heat flux from the μ-ILED. The temperature change in Fig. 2(b) is linearly proportional to the injection power and depends strongly on the size of μ-ILED. For example, for an injection power of 8.0 mW, the temperature change for the smallest μ-ILED ($100 \times 100\ \mu m^2$) is 97.6 K, which is more than 40 times larger than that for the largest μ-ILED ($1 \times 1\ mm^2$) (2.4 K), qualitatively consistent with previously reported results.[13,14]

The temperature change in Fig. 2(b) leads to a change in the bandgap according to $E_g = [3.47 - 7.7 \times 10^{-4} \times T^2/(T + 600)]$ eV,[20] where the temperature T (in K) is the sum of the ambient temperature and the temperature change ΔT in Fig. 2(b). The peak wavelength of emission is then obtained from $\lambda = hc/E_g$, where h is Planck's constant and c is the speed of light. For an ambient temperature of 298 K, Fig. 2(c) shows the change of the peak wavelength of emission for

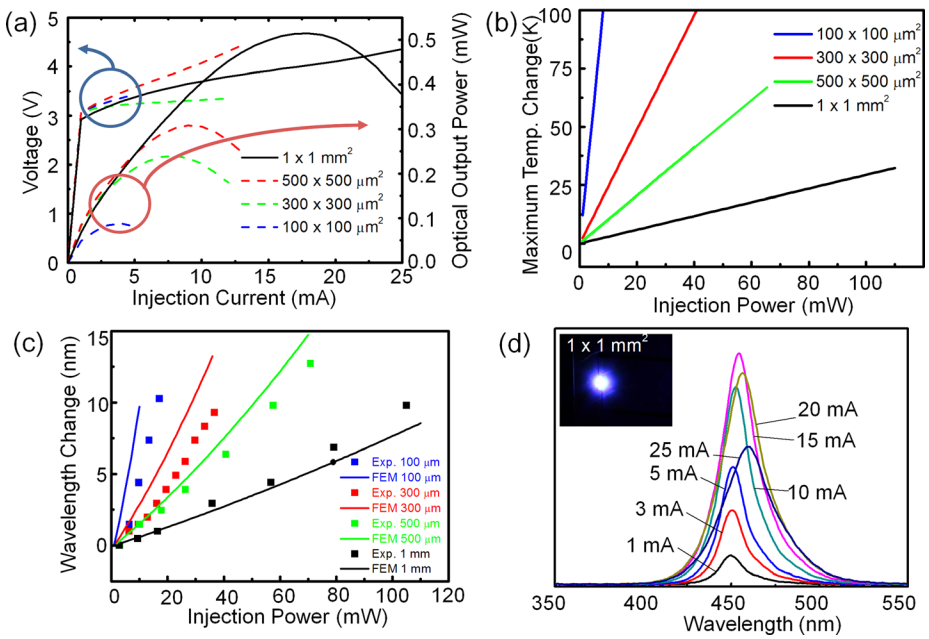

FIG. 2. (a) L-I-V curves, (b) estimated maximum temperature changes, and (c) experimental (dots) and FEM (lines) emission peak wavelength changes vs injection current of flexible μ-ILEDs with $100 \times 100\ \mu m^2$, $300 \times 300\ \mu m^2$, $500 \times 500\ \mu m^2$, and $1 \times 1\ mm^2$ chip sizes at 298 K. (d) shows the EL spectra of a $1 \times 1\ mm^2$ flexible μ-ILED with increasing the injection current from 1 to 25 mA at 298 K and the photograph of the emitted blue light. The inset of (d) shows image of a $1 \times 1\ mm^2$ μ-ILED transferred on the flexible substrate.

various device sizes as a function of injection power. The changes in peak wavelength obtained analytically (lines) based on the temperature of the μ-ILEDs in Fig. 2(b) agree reasonably well with experiment results (dots). The results can be explained by a competition between effects related to screening of the quantum confined Stark effect, band filling, and bandgap shrinkage by self-heating.[18,28,29] As shown in Fig. 2(c), the emission peak shifts to the red with increasing the injection power, for all samples. The peak wavelengths of emission are relatively high in smaller devices, due to the enhanced bandgap shrinkage and self-heating effects. The ratios of the emission peak wavelength shift to the injection current ($\Delta\lambda/\Delta$I) are 2.64, 1.09, 0.88, and 0.40 nm/mA for $100 \times 100\,\mu m^2$, $300 \times 300\,\mu m^2$, $500 \times 500\,\mu m^2$, and $1 \times 1\,mm^2$ devices, respectively. Fig. 2(d) shows the electroluminescence (EL) spectra of a 1×1 mm^2 μ-ILED with increasing injection current from 1 to 25 mA at 298 K. As the current increases, the EL intensity increases up to a maximum at 15 mA; further increases in current lead to decreases in EL. The emission peak wavelength and full width at half maximum (FWHM) increase with current from 449.79 nm and 16.68 nm at 1 mA ($J = 0.10\,A/cm^2$) to 459.58 nm and 34.19 nm at 25 mA ($J = 2.50\,A/cm^2$). A photograph of light emitted from a 1×1 mm^2 flexible μ-ILED appears in the inset of Fig. 2(d).

To study the effects of size dependent behaviors on plastic substrates, measurements at various temperatures defined by an external heating stage for normalized EL intensity, peak wavelength, and L-I-V properties were performed. Fig. 3(a) shows the normalized EL intensity for μ-ILEDs with different sizes as a function of temperature at an injection current of 5 mA. The temperature dependence of the EL intensity (I) can be approximated with a phenomenological form: $I = I_{T=298K} \exp[-(T - 298\,K)/T_1)$, where $I_{T=298K}$ is the emission intensity at 298 K, T is the heatsink temperature, and T_1 is a characteristic temperature. As shown in Fig. 3(a), the value of T_1 is 298.52 ($J = 50\,A/cm^2$), 313.46 ($J = 5.56\,A/cm^2$), 323.54 ($J = 2\,A/cm^2$), and 373.64 ($J = 0.5\,A/cm^2$) K for $100 \times 100\,\mu m^2$, $300 \times 300\,\mu m^2$, $500 \times 500\,\mu m^2$, and 1×1 mm^2 devices, respectively. As expected, T_1 decreases with decreasing device size, due to enhanced capacity for passive heat dissipation. These characteristics are consistent with the results of the L-I-V curves and emission peak wavelength shifts in Fig. 2(a). Fig. 3(b) shows the temperature-dependent L-I-V curves of a 1×1 mm^2 μ-ILED, for injection currents and temperatures between 0–25 mA and 298–358 K (10 K interval), respectively. The measured relationship between L and I shows that the slope efficiency ($\Delta P_{opt}/\Delta$I) gradually decreases with increasing injection current, due to the device heating.[30,31] The maximum P_{opt} and forward voltage decrease from 0.52 mW and 4.03 V to 0.39 mW and 3.89 V, respectively, as the temperature increases from 298 to 358 K. The turn-on voltage decreases from 2.93 V at 298 K to 2.74 V at 358 K. Fig. 3(c) shows the shift in the emission peak wavelength as a function of temperature at injection current levels of 3, 5, and 10 mA. At each current level, the wavelength red-shifts by an amount linearly proportional to the temperature, with a temperature coefficient of ~0.044 nm/K. Results shown in Fig. 3 demonstrate that temperature characteristics for μ-ILEDs on flexible plastic substrates are consistent with

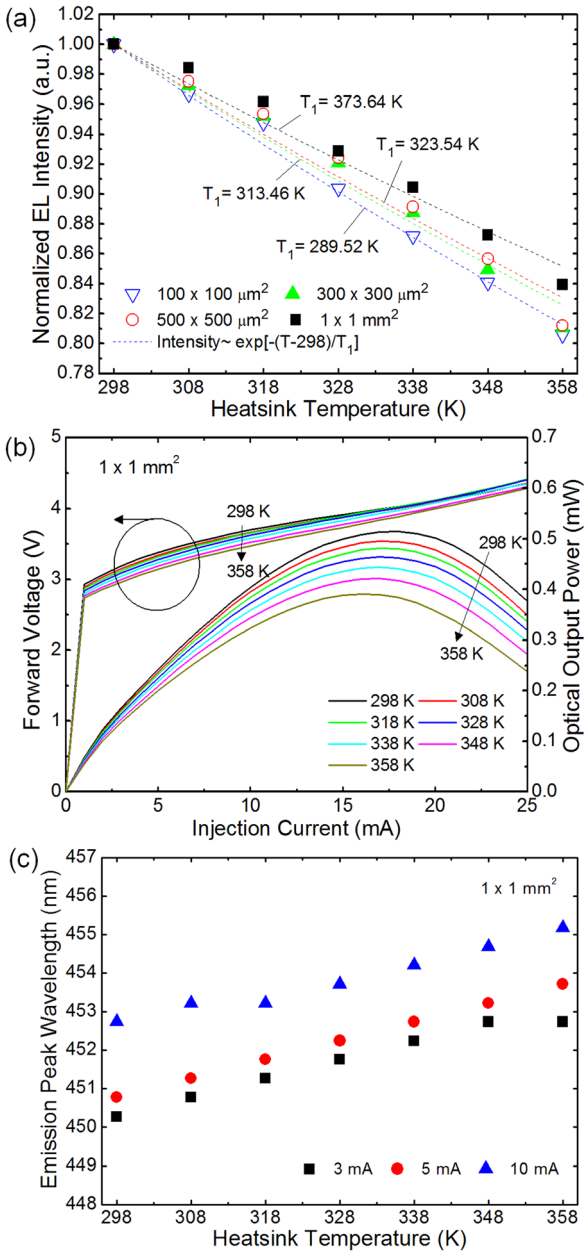

FIG. 3. (a) Normalized EL intensity of flexible μ-ILEDs with $100 \times 100\,\mu m^2$, $300 \times 300\,\mu m^2$, $500 \times 500\,\mu m^2$, and 1×1 mm^2 chip sizes as a function of temperature of a heating stage at an injection current of 5 mA. (b) Temperature-dependent L-I-V curves and (c) the emission peak wavelength shift as a function of temperature of the stage at injection current levels of 3, 5, and 10 mA for the flexible μ-ILED with 1×1 mm^2 chip size.

the findings summarized in Fig. 2. In other words, effects of heating and poor thermal dissipation cause red-shifting, optical power droop, and changes in I-V turn-on characteristics.

In summary, the results presented here reveal fundamental effects, optical, and spectral properties of flexible μ-ILEDs, and their temperature- and size-dependent device characteristics for $100 \times 100\,\mu m^2$, $300 \times 300\,\mu m^2$, $500 \times 500\,\mu m^2$, and 1×1 mm^2 chip sizes. These baseline data and the associated models can guide design of flexible inorganic optoelectronic devices for emerging applications, particularly those in bio-integrated devices for optogenetics, phototherapy and other areas where tight control of thermal behaviors is essential.

This research was supported by the Institute for Basic Science (IBS) (T.-i.K) and Basic Science Research Program through the National Research Foundation of Korea Grant funded by the Ministry of Science, ICT & Future Planning (2009-0083540), NRF-2013-R1A1A1061403 (T.-i.K.), and No. 2013-010037 (J.S.Y.) in Korea. Research was also supported by the US Department of Energy, Office of Basic Energy Sciences, Division of Materials Sciences and Engineering under Award DE-FG02-07ER46471 through the Frederick Seitz Materials Research Laboratory at the University of Illinois at Urbana–Champaign.

[1]D.-H. Kim, N. Lu, R. Ma, Y.-S. Kim, R.-H. Kim, S. Wang, J. Wu, S. M. Won, H. Tao, A. Islam, K. J. Yu, T.-I. Kim, R. Chowdhury, M. Ying, L. Xu, M. Li, H.-J. Chung, H. Keom, M. McCormick, P. Liu, Y.-W. Zhang, F. G. Omenetto, Y. Huang, T. Coleman, and J. A. Rogers, Science **333**, 838 (2011).
[2]T. Sekitani and T. Someya, MRS Bull. **37**, 236 (2012).
[3]G. Schwartz, B. C.-K. Tee, J. Mei, A. L. Appleton, D. H. Kim, H. Wang, and Z. Bao, Nat. Commun. **4**, 1859 (2013).
[4]M. S. White, M. Kaltenbrunner, E. D. Glowacki, K. Gutnichenko, G. Kettlgruber, I. Graz, S. Aazou, C. Ulbricht, D. A. M. Egbe, M. C. Miron, Z. Major, M. C. Scharber, T. Sekitani, T. Someya, S. Bauer, and N. S. Sariciftci, Nat. Photonics **7**, 811 (2013).
[5]T.-I. Kim, J. G. McCall, Y. H. Jung, X. Huang, E. R. Siuda, Y. Li, J. Song, Y. M. Song, H. A. Pao, R.-H. Kim, C. Lu, S. D. Lee, I.-L. Song, G. Shin, R. Al-Hasani, S. Kim, M. P. Tan, Y. Huang, F. G. Omenetto, J. A. Rogers, and M. R. Bruchas, Science **340**, 211 (2013); J. G. McCall, T.-I. Kim, G. Shin, X. Huang, Y. H. Jung, R. Al-Hasani, F. G. Omenetto, M. R. Bruchas, and J. A. Rogers, Nat. Protoc. **8**, 2413 (2013).
[6]J.-S. Park, H. Chae, H. K. Chung, and S. I. Lee, Semicond. Sci. Technol. **26**, 034001 (2011).
[7]H. Cao, L. Gu, S. K. Mohanty, and J.-C. Chiao, IEEE Trans. Biomed. Eng. **60**, 225 (2013).
[8]R.-H. Kim, D.-H. Kim, J. Xiao, B. H. Kim, S.-I. Park, B. Panilaitis, R. Ghaffari, J. Yao, M. Li, Z. Liu, V. Malyarchuk, D. G. Kim, A.-P. Le, R. G. Nuzzo, D. L. Kaplan, F. G. Omenetto, Y. Huang, Z. Kang, and J. A. Rogers, Nature Mater. **9**, 929 (2010).
[9]D. E. J. G. J. Dolmans, D. Fukumura, and R. K. Jain, Nat. Rev. Cancer. **3**, 380 (2003).
[10]S.-I. Park, Y. Xiong, R.-H. Kim, P. Elvikis, M. Meitl, D.-H. Kim, J. Wu, J. Yoon, C.-J. Yu, Z. Liu, Y. Huang, K.-C. Hwang, P. Ferreira, X. Li, K. Choquette, and J. A. Rogers, Science **325**, 977 (2009).
[11]R.-H. Kim, H. Tao, T.-I. Kim, Y. Zhang, S. Kim, B. Panilatis, M. Yang, D.-H. Kim, Y. H. Jung, B. H. Kim, Y. Li, Y. Huang, F. G. Fiorenzo, and J. A. Rogers, Small **8**, 2812 (2012).
[12]T.-I. Kim, R.-H. Kim, and J. A. Rogers, IEEE Photon J. **4**, 607 (2012).
[13]H. Kim, E. Brueckner, J. Song, Y. Li, S. Kim, C. Lu, J. Sulking, K. Choquette, Y. Huang, R. G. Nuzzo, and J. A. Rogers, Proc. Natl. Acad. Sci. U.S.A. **108**, 10072 (2011).
[14]T.-I. Kim, Y. H. Jung, J. Song, D. Kim, Y. Li, H.-S. Kim, I.-S. Song, J. J. Wierer, H. A. Pao, Y. Huang, and J. A. Rogers, Small **8**, 1643 (2012).
[15]Y. Jung, X. Wang, J. Kim, S. H. Kim, F. Ren, S. J. Rearton, and J. Kim, Appl. Phys. Lett. **100**, 231113 (2012).
[16]J. Chun, T. Hwang, Y.-S. Choi, T. Jeong, J. H. Baek, H. C. Ko, and S.-J. Park, IEEE Photon. Lett. **24**, 2115 (2012).
[17]A. Carlson, A. M. Bowen, Y. Huang, R. G. Nuzzo, and J. A. Rogers, Adv. Mater. **24**, 5284–5318 (2012).
[18]Z. Gong, S. Jin, Y. Chen, J. McKendry, D. Massoubre, I. M. Watson, E. Gu, and M. D. Dawson, J. Appl. Phys. **107**, 013103 (2010).
[19]Y. D. Jhou, C. H. Chen, R. W. Chuang, S. J. Chang, Y. K. Su, P. C. Chang, P. C. Chen, H. Hung, S. M. Wang, and C. L. Yu, Solid-State Electron. **49**, 1347 (2005).
[20]M. E. Levinshtein, S. L. Rumyantsev, and M. S. Shur, *Advanced Semiconductor Materials GaN, AlN, LnN, BN, SiC, SiGe* (John Wiley & Sons, NY, 2001).
[21]H. Ünlü, Solid-State Electron. **35**, 1343 (1992).
[22]ABAQUS Analysis User's Manual V6.9, Dassault Systemes, Pawtucket, 2009.
[23]C. Lü, Y. Li, J. Song, H. S. Kim, E. Brueckner, B. Fang, K. C. Hwang, Y. Huang, R. G. Nuzzo, and J. A. Rogers, Proc. R. Soc. A **468**, 3215 (2012).
[24]Y. Li, Y. Shi, J. Song, C. Lü, T.-I. Kim, J. A. Rogers, and Y. Huang, J. Appl. Phys. **113**, 144505 (2013).
[25]R. Li, Y. Li, C. Lü, J. Song, R. Saeidpouraza, B. Fang, Y. Zhong, P. M. Ferreira, J. A. Rogers, and Y. Huang, Soft Matter **8**, 7122 (2012).
[26]D. Erckson, D. Sinton, and D. Li, Lab Chip **3**, 141 (2003).
[27]F. P. Incropera, D. P. DeWitt, T. L. Bergman, and A. S. Layine, *Fundamentals of Heat and Mass Transfer* (Wiley, Hoboken, 2007).
[28]Y. F. Wu, H. P. Hsu, and T. Y. Liu, Solid-State Electron. **68**, 63 (2012).
[29]E. J. Jung, S. J. Kim, and H. S. Kim, Curr. Appl. Phys. **12**, 885 (2012).
[30]J. Xie, X. Ni, Q. Fan, R. Shimada, U. Ozgur, and H. Morkoc, Appl. Phys. Lett. **93**, 121107 (2008).
[31]J. Yan, T. J. Yu, X. B. Li, Y. B. Tao, C. L. Xu, H. Long, Z. Y. Yang, and G. Y. Zhang, J. Appl. Phys. **110**, 073102 (2011).